Journal of Thermal Analysis, Vol. 50 (1997) 533-545

MODELLING THE KINETICS OF SOLUTE SEGREGATION TO PARTIAL DISLOCATIONS FOR ISOTHERMAL MICROCALORIMETRIC EVALUATIONS

A. Varschavsky and E. Donoso

Universidad de Chile, Facultad de Ciencias Físicas y Matemáticas, Instituto de Investigaciones y Ensayes de Materiales (IDIEM), Casilla 1420, Santiago, Chile

(Received October 15, 1996)

Abstract

A model is proposed to describe the kinetics of solute segregation to partial dislocations in solid solutions of cold-rolled alloys. The case when half edge and half screw dislocations are present is considered. The model gives account of the kinetic behaviour observed in a deformed Cu-19 at% Al alloy where two unknown processes could be assessed during calorimetric isothermal experiments. The faster process corresponds to segregation to screw dissociated dislocations while the slower one corresponds to segregation to edge dissociated dislocations. Experimental activation energies, larger for edge dislocations, are close to that for pipe diffusion along the partials corrected by pinner binding energy terms. It is also predicted that segregation occurs faster as the dislocation density is increased. A quantitative comparison of experimental results with model predictions is given.

Keywords: Cu-19 at% Al, dislocations, kinetics, segregation

Introduction

It is well known that in solid solutions of cold-worked Cu annealed below the recrystallization temperature, a hardening effect [1–4] called anneal hardening [5–11] is produced due particularly to the interaction of solute atoms with lattice defects. This effect may cause a considerable increase in flow stress, in which solute locking to dislocations plays the most important role [12, 13], although solute segregation to stacking faults may not be disregarded [14].

The above phenomenon is important not only in the elucidation of the hardening mechanism, but it is also of primary interest for studies of static [15] and dynamic strain ageing [15–18] and also for strain sensitivity determinations. Most works on solute-dislocation interactions do not take into account two main effects that characterize Cu solid solutions, namely: a) the fact that dislocations are dissociated and b) the distribution character of extended dislocations, sensitive to the deformation mode (rolling, drawing, torsion, flexion, etc.).

0368–4466/97/ $ 5.00

John Wiley & Sons Limited
Chichester

We have modelled solute-dislocation pinning effects in a recent paper [19], testing qualitatively the hypothesis that this is the main cause of the predominant hardening mechanism. The model was based on energetic considerations taking into account the above mentioned a) and b) alloy features. Such an energetic approach is very suitable with differential scanning calorimetry (DSC) as an effective experimental tool for assessing dislocation densities and energy balance compatible with the segregation process.

As it is important to examine the kinetics of solute anchoring to partial dislocations in deformed Cu solid solutions, the present work chiefly discloses a model based on the previous one as a starting point for predicting the kinetics of the pinning process and for testing its validity in Cu-19 at% Al using isothermal microcalorimetric experiments.

Segregation kinetics

A previous work [19] established that the energy $\Delta H_d(\Phi)$ evolved during segregation of solute atoms to partial dislocations with a probability density function $f(\Phi)$ ascribed to a dislocation character Φ is given by:

$$\Delta H_d(\Phi) = \frac{\pi \rho b^2}{c} \int_c^{\pi/2} f(\Phi) \, [\Delta H_{a1}(\Phi) c_{d1}(\Phi) + \Delta H_{a2}(\Phi) c_{d2}(\Phi)] \, d\Phi \tag{1}$$

where ρ is dislocation density, b is Burger's vector, c is alloy composition; $\Delta H_{a1}(\Phi)$, $\Delta H_{a2}(\Phi)$ and $c_{d1}(\Phi)$, $c_{d2}(\Phi)$ are binding energies and equilibrium solute concentrations in the leading and trailing partials, respectively.

In particular it was shown for cold-rolled copper solid solutions [4, 19] that a bimodal-extreme-discrete distribution where half edge and half screw dissociated dislocations are present is suitable to describe the evolved energy associated with the segregation process, that is

$$\Delta H_d = \frac{\pi \rho b^2}{c} [\Delta H_{ac} c_{de} + \Delta H_{as} c_{ds}] \tag{2}$$

where subscripts e and s refer to edge and screw dislocations, respectively.

During segregation the evolved heat $\Delta H(t)$ at time t is a function of kinetic paths of solute concentrations $c_e(t)$ and $c_s(t)$ of edge and screw dislocations before equilibrium values c_{de} and c_{ds} are attained, expressed as:

$$\Delta H(t) = \frac{\pi \rho b^2}{c} [\Delta H_{ae} c_e(t) + \Delta H_{as} c_s(t)] \tag{3}$$

The effective solute composition at arrested dislocations is determined by the ageing time of the dislocations. A number of models have been designed, based

on diffusion and drift of solute in the stress fields of dislocations in order to explain the various time dependences found. Assuming a general Cottrell-Bilby solute concentration kinetics as a starting point [20]:

$$c_e(t) = c(K_e Dt)^n \tag{4}$$

and

$$c_s(t) = c(K_s Dt)^n \tag{5}$$

where D is the effective solute diffusion coefficient of the underlying process, while K_e and K_s are constants depending on solute-dislocation binding energy. In the original Cottrell-Bilby model n=2/3. These expressions are valid only for the early stages of segregation. If a Louat's [21] correction of the general Cottrell-Bilby analysis used here to include saturation at longer ageing times is applied, that is, when the maximum number of pinners that may be accommodated in the dislocation core is considered, Eqs (4) and (5) become

$$c_e(t) = c_{de}\left[1-\exp\left(-\frac{c(K_e Dt)^n}{c_{de}}\right)\right] \tag{6}$$

and

$$c_s(t) = c_{ds}\left[1-\exp\left(-\frac{c(K_s Dt)^n}{c_{ds}}\right)\right] \tag{7}$$

As a first approximation, in order to express Eqs (5) and (7) in a Mehl-Johnson-Avrami form, equilibrium concentrations are considered to be governed by Boltzmann statistics, and for the present case they are:

$$c_{de} = c\exp\left(-\frac{\Delta H_{ae}}{RT}\right) \tag{8}$$

and

$$c_{ds} = c\exp\left(-\frac{\Delta H_{as}}{RT}\right) \tag{9}$$

With the above assumptions and considering $D=D_o\exp(-Q/RT)$, D_o being the diffusion

$$\Delta H(t) = \frac{\pi\rho b^2}{c}\left(\Delta H_{ae}c_{de}\left(1-\exp\left[-\left(\frac{t}{\tau_e}\right)^n\right]\right)+\Delta H_{as}c_{ds}\left(1-\exp\left[-\left(\frac{t}{\tau_s}\right)^n\right]\right)\right) \tag{10}$$

where

$$\tau_e = \frac{1}{K_e D_o} \exp\left(\frac{Q - \frac{1}{n}\Delta H_{ae}}{RT}\right) \tag{11}$$

and

$$\tau_s = \frac{1}{K_s D_o} \exp\left(\frac{Q - \frac{1}{n}\Delta H_{as}}{RT}\right) \tag{12}$$

the activation energies for both processes being $Q-(1/n)\Delta H_{ae}$ and $Q-(1/n)\Delta H_{as}$, $\tau_{oe}=1/K_e D_o$ and $\tau_{os}=1/K_s D_o$. If the reacted fraction associated with the process is defined by:

$$y = \frac{\Delta H(t)}{\Delta H_d} \tag{13}$$

Eqs (2) and (10) yield the convex linear combination:

$$y = \psi\left(1-\exp\left[-\left(\frac{t}{\tau_e}\right)^n\right]\right) + (1-\psi)\left(1-\exp\left[-\left(\frac{t}{\tau_s}\right)^n\right]\right) \tag{14}$$

or

$$1 - y = \psi \exp\left[-\left(\frac{t}{\tau_e}\right)^n\right] + (1-\psi)\exp\left[-\left(\frac{t}{\tau_s}\right)^n\right] \tag{15}$$

with

$$\psi = \frac{\Delta H_{ae} c_{de}}{\Delta H_{ae} c_{de} + \Delta H_{as} c_{ds}} \tag{16}$$

Hence, the present model predicts that two processes with different relaxation times are involved in segregation kinetics. Since the reacted fraction is based on heat measurements, it is very suitable for DSC evaluation.

Numerical results concerning Cu-19 at% Al

This section analyses DSC and isothermal calorimetric trace features in a deformed αCu–Al alloy in connection with the segregation kinetic model proposed herein. The Cu–Al alloy used was chemically analyzed and found to contain 9.0±0.1 wt%, 19 at% aluminium. It was prepared in a Batlzers VSG 10 vacuum induction furnace from electrolytic copper (99.95 wt%) and aluminium (99.97 wt%) in a graphite crucible. The ingot was subsequently hot forged at 923 K to a thickness of 10 mm, pickled to remove oxide from the surface, an-

nealed in a vacuum furnace at 1123 K for 36 h to achieve complete homogeneity, and cooled in the furnace to room temperature. It was then cold rolled to 1.5 mm thickness with intermediate anneals at 873 K for one hour. After the last anneal the material was heat treated at 873 K, furnace cooled at a rate of 5 K h^{-1} and finally cold rolled to 0.75 mm thickness (50% reduction).

Microcalorimetric analysis of the samples was performed in a DuPont 2000 thermal analyzer. Specimen discs of 0.75 mm thickness and 6 mm diameter were prepared. To increase measurement sensitivity, a high-purity and well-annealed copper discs, in which no thermal events occur in the temperature range employed, was used as a reference. To minimize oxidation, dried nitrogen (0.8×10^{-4} m^3 min^{-1}) was passed through the calorimeter.

DSC curves

A material slowly cooled in the furnace was chosen in the present case, because prior to cold work it is in a highly ordered state, determined by the equilibrium value of the first short-range-order (SRO) parameter at freezing temperature [22]. After deformation the alloy gets disordered to an extent readily determined [19], along with the creation of excess vacancies. On heating, reordering of the alloy takes place to a degree of order determined by the equilibrium value of the first SRO parameter at the final temperature of stage 1 of the DSC trace shown in Fig. 1a. Stage 2, which overlaps stage 1, corresponds to segregation of solute to partial dislocations [19], while stage 3 corresponds to a disordering process [2, 22–24] somewhat overlapping with stage 4 corresponding to recrystallization [2, 25]. A pre-anneal of 20 min at a temperature lower than the peak temperature of stage 1, at which stage 2 still does not start, anneals-out the reordering effect present in Fig. 1a, as shown in Fig. 1b. Hence, the segregation peak can be clearly isolated. It should be emphasized that a low heating rate was em-

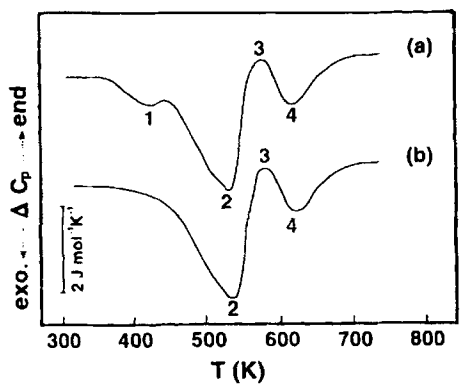

Fig. 1 DSC traces on heating at 0.08 K s^{-1} for: a) furnace cooled and cold-rolled Cu-19 at% Al; b) furnace cooled, cold-rolled and pre-annealed material

ployed in order to minimize the overlapping effect produced as the heating rate is increased, thus avoiding simultaneous reactions (order and segregation) at temperatures chosen for isothermal runs. In this way these two non-isothermal runs allow selection of the temperature range of isothermal experiments using samples pre-annealed at 430 K. It is worth recalling that non-isothermal runs were unsuccessful in detecting two processes during segregation, even at very low heating rates. Only weak evidences that a complex reaction associated with stage 2 is taking place can then be noticed.

Isothermal microcalorimetry

DSC outputs for isothermal segregation are shown in Fig. 2. The temperature range for these experiments was chosen between 450 and 530 K. In order to make the experimental results compatible with the segregation model proposed, it will be assumed that equation:

$$1 - y = A \exp\left[-\left(\frac{t}{\tau_1}\right)^n\right] + (1-A) \exp\left[-\left(\frac{t}{\tau_2}\right)^n\right] \tag{17}$$

is valid with different time constants τ_1, τ_2 and with parameters A and $(1-A)$ as cofactors, and with the same time exponent n for both processes. In order to search for the time exponent, selected values of n were tried. By making variable changes $t^*=t^n$, $\tau_1^*=\tau_1^n$ and $\tau_2^*=\tau_2^n$ and using Eqs (4), (5), (6) and (7) of Ref. [26], τ_1, τ_2 and A can be determined for each n tested. After employing n=1/3, 2/5, 1/2,

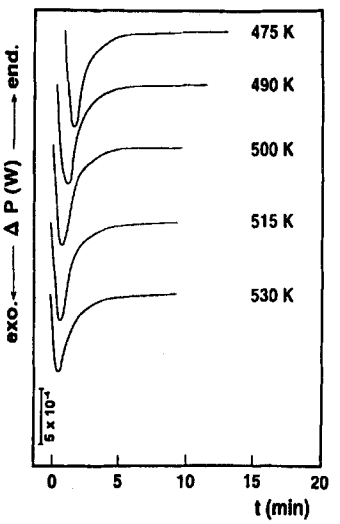

Fig. 2 DSC traces for isothermal solute segregation to partial dislocations at the indicated temperatures for furnace cooled, cold-rolled and pre-annealed Cu-19 at% Al alloys

2/3, 3/5, 3/4 and 1, the best fit to the experimental curves was obtained for n=2/5. The corresponding τ_1, τ_2 and A values are listed in Table 1 for various annealing temperatures.

Table 1 Values of time constants τ_1, τ_2 and parameter A for n=2/5 at different annealing temperatures T

T/K	τ_1/min	τ_2/min	A
475	15.64	6.05	0.70
490	6.30	2.86	0.687
500	3.81	1.57	0.675
515	1.65	0.82	0.665
530	0.91	0.45	0.66

The corresponding $(1-y)$ functions *vs.* $t^{2/5}$ (solid lines) plotted in Fig. 3 agree satisfactorily with the experimental points extracted from the traces. Data points from DSC outputs for the very early stages of the segregation reactions, where some departures of the two exponential laws are observed, were omitted in the numerical analysis. The $\ln(1-y)$ *vs.* $t^{2/5}$ curves in Fig. 4 show that a single exponential law is followed for longer times, while there is a superposition of two processes for short annealing times, the first process being more rapid than the other one, which is dominating for longer times.

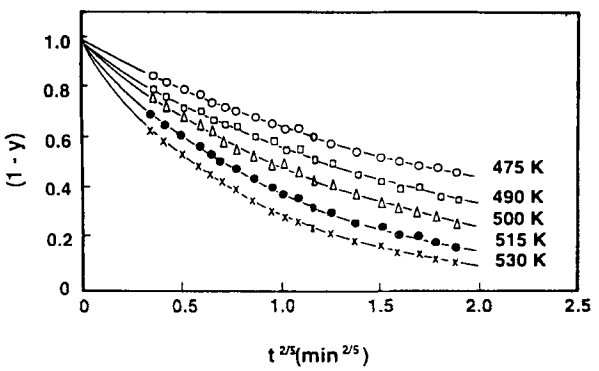

Fig. 3 $(1-y)$ *vs.* $t^{2/5}$ curves at the indicated temperatures

To get a numerical insight into the temperature dependence of the two processes, an Arrhenius equation was set up for relaxation times τ_1 and τ_2. From plots of $\ln\tau_1$ and $\ln\tau_2$ *vs.* $1/T$ shown in Fig. 5, the corresponding activation energies E_1, E_2 and the respective specific time constants τ_{o1}, τ_{o2} were determined, giving E_1= 110.3 kJ mol^{-1}, E_2=100.1 kJ mol^{-1}, $\tau_{o1}=3.4\times10^{-11}$ min and $\tau_{o2}=1.5\times10^{-10}$ min.

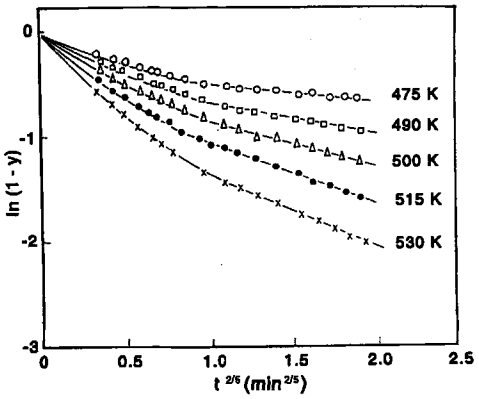

Fig. 4 Ln(1–y) *vs.* $t^{2/5}$ curves at the indicated temperatures

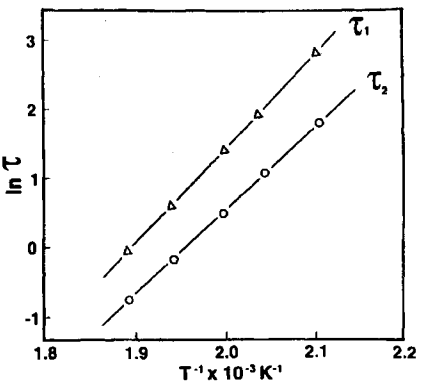

Fig. 5 Ln τ *vs.* $1/T$ plots for the two processes taking place during solute segregation to partial dislocations in Cu-19 at% Al

It is interesting to note that the activation energy from Kissinger plots, (not shown here for brevety's sake) obtained from non-isothermal traces at different heating rates, gives for stage 2 a value of 106.3 kJ mol^{-1} close to the higher value obtained from the isothermal runs for the two processes. The fact that the two processes cannot be separated in non-isothermal experiments is probably due to lack of sufficient resolution.

Discussion

To analyze the experimental values of activation energy it is necessary to consider that diffusion enhancement due to deformation is reflected by pipe diffusion along dislocations. Pipe diffusion may result because, after the deforma-

tion process, a gliding dislocation arrested by a less mobile forest dislocation will now mainly increase its solute concentration by the passage of solutes from the more anchored forest to the less anchored gliding dislocation. Thus, the effective diffusion coefficient can be written as:

$$D = D_p g + D_b(1 - g) \tag{18}$$

where D_p is the pipe diffusion coefficient, D_b is the lattice diffusion coefficient, and g is atom fraction associated with the pipe. Assuming that the dislocation core cross-section contains 2 atoms

$$g = \frac{2\Omega_o \rho}{b_p} \tag{19}$$

in which Ω_o is the atomic volume and b_p=0.58 b is the Burger's vector of a partial edge or screw dissociated dislocation. Even for extremely high dislocation densities g<<1 giving D=$D_p g$+D_b. At temperatures below half the melting point, where most of the segregation takes place, $D_p g$ can be much greater than D_b [27], thereby yielding $D \approx D_p g$, or

$$D = \frac{2\Omega_o \rho}{b_p} D_{ob} \exp\left(-\frac{Q_p}{RT}\right) \tag{20}$$

where the activation energy for pipe diffusion Q_p was taken similar to that of grain boundary diffusion [11] which in turn is a little more than half of that for volume diffusion $Q_b \approx 162.8$ kJ mol^{-1} [28]. On the other hand, the pre-exponential factor of D_p, can be taken from lattice diffusion $D_{op} \approx D_{ob}$=6.68×10^{-5} m^2 s^{-1} [29]. For instance, at 530 K, which is the higher temperature employed in isothermal runs, taking Ω_o=7.1×10^{-30} m^3, b=2.6×10^{-10} m and ρ=4.6×10^{15} m^{-2} [19] from a previous work, one obtains in principle D/D_b=1.57×10^5 thus making very likely that most of the diffusion takes place along dislocations.

The activation energy for pipe diffusion was estimated as Q_p=81.4 kJ mol^{-1} [28]. However, if the binding energy is not negligible, then the solute can change the pipe structure, for example fill in open spaces and make it harder for atoms to move along the dislocations (pinner effects). This effect cannot be quantified so simply, and there is no widely accepted theory on solute diffusion or on the effect of solutes on solvent diffusion, as there is for lattice diffusion. The above effect should produce an increase in effective activation energy, as predicted by the present model which depends on the magnitude of binding energy (edge or screw dissociated dislocations) and on the time exponent provided all segregation occurs by atom flux along the pipes. Thus, Eqs (11) and (12) yield for the effective activation energy for pipe diffusion with n=1/3 [30]:

$$E_{ep} = Q_p - 3\Delta H_{ae} \tag{21}$$

for edge and

$$E_{sp} = Q_p - 3\Delta H_{as} \tag{22}$$

for screw dislocations. It is expected that in the very early stages of the process when solute concentration at dislocations is far from its saturation value, pinned solute atom effects will not contribute to the activation energy, regardless of the dislocation character as predicted by Eqs (4) and (5) with $D=D_p$ [21].

Since the previously calculated values for the solute-dislocation binding energies are $\Delta H_{ae}=-8.40$ kJ mol^{-1} and $\Delta H_{as}=-4.84$ kJ mol^{-1} [19], it follows that $E_{ep}=101.1$ kJ mol^{-1} and $E_{sp}=92.2$ kJ mol^{-1}, which values are about 10 and 4% lower than the measured experimental values E_1 and E_2, respectively. In turn, E_1 and E_2 are a little more than half the effective activation energies for volume diffusion which from Eqs (11) and (12) yield:

$$E_{eb} = Q_b - \frac{3}{2}\Delta H_{ae} \tag{23}$$

for edge, and

$$E_{sb} = Q_b - \frac{3}{2}\Delta H_{as} \tag{24}$$

for screw dislocations, with $n=2/3$ [20]. Values of E_1 and E_2 are still much lower than $E_{eb}=E_{sb}$ even if pinner effects are disregarded. Therefore one can further infer that E_1 and E_2 correspond to the experimental apparent measured activation energies for solute segregation to edge and screw dislocations, respectively, where mainly pipe diffusion takes place.

It is worth recalling that already pinned solute atoms are stronger obstacles to solute movement inside the dislocation core for a pipe ($-3\Delta H_{ae}$, $-3\Delta H_{as}$) than for a bulk ($-3/2\Delta H_{ae}$, $-3/2\Delta H_{as}$) diffusion mechanism regardless of the dislocation character, pinner effects being always larger for edge dislocations.

The experimental apparent activation energy Q_{app} for solute segregation in the early stages of pinning can now be evaluated. From the measured values E_1 and E_2 and n and considering that:

$$E_1 = Q_{app} - \frac{5}{2}\Delta H_{ae} \tag{25}$$

and

$$E_1 = Q_{app} - \frac{5}{2}\Delta H_{as} \tag{26}$$

one obtains $Q_{app}=89.3$ kJ mol^{-1} from Eq. (25) and 88.0 kJ mol^{-1} from Eq. (26), which, as expected, are in excellent agreement, differing by less than 1%. Note that Q_{app} is a little larger than Q_p, but much smaller than Q_b, thus reflecting that

the prevailing mechanism for solute segregation in this alloy after 50% cold rolling is pipe diffusion.

As said before in the present study, an experimental time exponent n=2/5 was found. It was also mentioned previously that for bulk diffusion and short times n=2/3 has been derived [20]; an analogous argument applied to pipe diffusion yields n=1/3 [31]. The long time approximation for bulk and pipe diffusion including concentration gradients, leads to n=1/2 [32]. The exponent 2/3 for bulk diffusion is a consequence of the fact that during the time t, solute from a distance of up to r may diffuse to the dislocation. For sufficiently short times the diffusion distance r increases as $r \propto (Dt)^{1/3}$ (D=diffusion constant) [20]. In the case of free diffusion in volume only, solutes inside a tube of radius r enclosing the dislocation core can arrive at it within t. The volume of the tube being proportional to r^2, the line concentration of solutes pinned increased proportionally to $t^{2/3}$. It follows that n=2/3 . In the case of pipe diffusion, the diffusion path is restricted to a line. Hence, not the whole volume of the enclosing tube proportional to $r^2 \propto t^{2/3}$ is the possible source for solute diffusion within t; instead, only the whole number of forest lines up to a length $r \propto t^{1/3}$ ending at the dislocation provide diffusion. Such a mechanism results in n=1/3 [31]. Specific questions concerning n have been recently discussed [30, 33–35]. The value n=1/3 has also been occasionally reported in the literature for aluminium alloys [16, 17]. For these alloys only one process is expected to take place in the process of segregation [16, 17], because of their high stacking fault energy which prevents dislocations from dissociating. The value n=2/5 here found might be consistent with a mechanism of pipe diffusion, in conjunction with some bulk diffusion in the later stages when pipes tend to be exhausted; both mechanisms affected by the already solute-pinned atoms, consistently with the activation energy analysis.

The constants K_e and K_s in Eqs (11) and (12) are proportional to the binding energies ΔH_{ae} and ΔH_{as} [18, 21], so that τ_{oe}/τ_{os}=0.576 which is comparable with the experimental ratio τ_{o1}/τ_{o2}=0.223, being within the same order of magnitude. Since from Eq. (20) one can take as a first approximation for the effective diffusion constant

$$D_o = \left(\frac{2\Omega_o \rho D_{ob}}{b_p} \right) \tag{27}$$

setting the measured values $\tau_{o1}=\tau_{oe}(=3.4\times10^{-11}$ min) and $\tau_{o2}=\tau_{os}(=1.5\times10^{-10}$ min), gives $K_e=1.02\times10^{18}$ m^2 and $K_s=2.31\times10^{17}$ m^2 for the alloy under study. These values differ by almost one order of magnitude from those theorectically predicted for bulk diffusion [18] and although higher, they lie whithin the same order of magnitude of those for pipe diffusion [30] in the range of temperatures employed. It is difficult to attain a higher degree of accuracy probably due to the range of values which D_o can assume arising from a certain degree of flexibility which exists in the choice of ρ and D_{ob}. However, the values found for τ_{o1} and τ_{o2} seem quite reasonable. It is also worth noting from Eqs (11),

(12) and (27) that the larger the dislocation density, the lower the expected values of τ_{oe} and τ_{os}, thus contributing to the enhancement of the kinetic process.

Regarding the experimental values of the constant A, they are somewhat lower than those of Ψ calculated from Eqs (8), (9) and (10), giving 0.80/0.79/0.782/ 0.775/0.765 for the corresponding temperatures of 475/490/500/515/530 K. This might be attributed to the choice of a Boltzmann distribution for c_{de} and c_{ds} as a first approximation, to achieve a more tractable sigmoidal behaviour for $c_e(t)$ and $c_s(t)$. In fact, if a Fermi distribution [19] is used for c_{de} and c_{ds} only to evaluate Ψ, values of 0.748/0.73/0.719/0.71/0.70 are obtained, which are closer to the experimental values of A.

Finally, the model developed herein is based on previous energetic results (19), predicting that half edge and half screw dislocations are present (Eq. (2)), and the observed kinetic behaviour confirms that such dislocation distribution characterizes cold-rolled Cu-19% Al.

Conclusions

This study leads to the conclusion that the disclosed model predicting two processes in the kinetics of solute segregation to partial dislocations during isothermal experiments, shows that these processes actually occur in a cold-rolled Cu-19 at% Al. It can also confirm that half edge and half screw dislocations are present during this deformation mode. The segregation rates increase with the dislocation density and are larger for screw than for edge dislocations. Most of the segregation takes place by pipe diffusion along the partials.

* * *

The authors would like to thank the Fondo de Desarrollo Científico y Tecnológico (FONDECYT) for financial support through Project 1950566, and the Instituto de Investigaciones y Ensayes de Materiales (IDIEM), Facultad de Ciencias Físicas y Matemáticas, Universidad de Chile, for the facilities provided for this research.

References

1 R. W. Cahn and R. G. Davies, Phil. Mag., 5 (1960) 119.
2 J. M. Popplewell and J. Crane, Metall. Trans., 2 (1971) 3411.
3 A. Varschavsky, Mater. Sci. Eng., 89 (1978) 118.
4 A. Varschavsky, J. Mater. Sci., 26 (1991) 3603.
5 M. Z. Butt and Z. Rafi, J. Mater. Sci. Letts., 10 (1991) 309.
6 A. Varschavsky and E. Donoso, Mater. Sci. Eng., 32 (1978) 65.
7 E. Donoso and A. Varschavsky, Mater. Sci. Eng., 37 (1979) 151.
8 A. Varschavsky and E. Donoso, Mater. Sci. Eng., 40 (1979) 119.
9 S. Fan, K. Inai, S. Onaka and S. Miura, J. Soc. Mater. Sci. Jpn., 41 (1992) 607.
10 A. Varschavsky and E. Donoso, Res Mechanica, 3 (1981) 195.
11 M. Militzer, W. P. Sun and J. J. Jonas, Acta Metall. Mater., 42 (1994) 133.
12 M. Z. Butt, Sci. Int., 2 (1990) 257.

13 F. R. N. Nabarro, Acta Metall. Mater., 38 (1990) 161.
14 A. Varschavsky, Scr. Metall., 9 (1975) 391.
15 L. P. Kubin, Y. Estrin and C. Perrier, Acta Metall. Mater., 40 (1992) 1037.
16 C. P. Ling, P. G. McCormick and Y. Estrin, Acta Metall. Mater., 41 (1993) 3323.
17 P. G. McCormick and P. Ling, Acta Metall. Mater., 43 (1995) 1969.
18 Y. Brechet and Y. Estrin, Acta Metall. Mater., 43 (1995) 955.
19 A. Varschavsky and E. Donoso, J. Thermal. Anal., 48 (1997) 1307.
20 A. H. Cottrell and B. A. Bilby, Proc. R. Soc. Lond., B62 (1949) 229.
21 N. Louat, Scripta Metall., 15 (1981) 1167.
22 A. Varschavsky and M. Pilleux, Mater. Letts., 17 (1993) 364.
23 A. Varschavsky and E. Donoso, Mater. Sci. Eng., A145 (1991) 95.
24 A. Varschavsky and E. Donoso, Metall. Trans., 15A (1984) 1999.
25 N. Kuwano, Y. Tomokiyo, C. Kinoshita and T. Eguchi, Trans. Jpn. Inst. Met., 15 (1974) 338.
26 P. Kittl and E. Donoso, J. Mater. Sci., 16 (1981) 533.
27 I. Dutta and D. L. Bourell, Acta Metall. Mater., 38 (1990) 2041.
28 G. Veith, L. Trieb, W. Püschl and H. P. Aubauer, Phys. Stat. Sol., 27 (1975) 59.
29 A. Varschavsky and E. Donoso, J. Mater. Sci., 21 (1986) 3873.
30 J. Schlipf, Scripta Metall. Mater., 29 (1993) 287.
31 F. Springer and Ch. Schwink, Scripta Metall. Mater., 25 (1991) 2739.
32 F. R. Brotzen and A. Seeger, Acta Metall., 37 (1989) 2985.
33 J. Schlipf, Scripta Metall. Mater., 31 (1994) 909.
34 A. Kalk, A. Nortmann and Ch. Schwink, Phil. Mag. A, 72 (1995) 1239.
35 M. A. Morris, T. Lipe and D. G. Morris, Scripta Mater., 34 (1996) 1337.